

Single-crystal structure refinements and crystal chemistry of synthetic trioctahedral micas $\text{KM}_3(\text{Al}^{3+}, \text{Si}^{4+})_4\text{O}_{10}(\text{OH})_2$, where $\text{M} = \text{Ni}^{2+}, \text{Mg}^{2+}, \text{Co}^{2+}, \text{Fe}^{2+}$, or Al^{3+}

GÜNTHER J. REDHAMMER* AND GEORG ROTH

Institute of Crystallography, Rheinisch-Westfälische Technische Hochschule Aachen, Jägerstrasse 17/19, D-52056 Aachen, Germany

ABSTRACT

To study structural changes with changing chemical composition in the octahedral sheet of trioctahedral potassium-rich 1M micas, 3 natural and 12 synthetic micas were examined by single-crystal X-ray diffraction. Samples with Ni^{2+} , Mg^{2+} , Co^{2+} , Fe^{2+} , and Al^{3+} in the octahedral sheet and with Si^{4+} , Al^{3+} and one sample with Ga^{3+} in the tetrahedral sheet were prepared at high temperatures and pressures, which yielded crystallites $\leq 200 \mu\text{m}$ in size. For samples with approximately AlSi_3 composition of the tetrahedral sheet and with no octahedral Al^{3+} , mean M1-O and M2-O octahedral bond lengths correlate very well with the mean ionic radius of the octahedral cations. For these samples, the M1 and M2 sites are found to be very similar or identical within experimental error in terms of mean M-O bond lengths, bond angles, and polyhedral distortion parameters. Octahedral distortion is negatively correlated with the size of the octahedral cation. Octahedra in Ni^{2+} -mica show the largest deviation from ideal octahedral geometry, whereas those in annite are closest to ideal octahedral geometry, but they are still significantly flattened. Octahedral Al^{3+} prefers the M2 site. This causes the mean M1-O bond length to decrease less with increasing Al^{3+} content as compared to the mean M2-O distance. This Al^{3+} preference for M2 also causes the M2 site to become smaller and more distorted than the M1 site. Refinement of the Mg-Fe ratios in the octahedral sites along the annite-phlogopite join shows that the two cations are statistically distributed over M1 and M2. Tetrahedra are regular and show only a small elongation along c^* . Tetrahedral distortion parameters for the AlSi_3 micas show no correlation with chemistry of the octahedral layer. However, the mean T-O bond lengths increase slightly with increasing size of the octahedral cation. With decreasing size of the lateral dimension of the octahedral sheet in the (001) plane, the tetrahedral sheet shows increasing ditrigonal distortion. Largest tetrahedral rotation angles are observed for synthetic near end-member siderophyllite with $\alpha = 11.5^\circ$ and for tetra-gallium-phlogopite $\text{KMg}_3\text{GaSi}_3\text{O}_{10}(\text{OH})_2$ with $\alpha = 10.8^\circ$.

INTRODUCTION

Trioctahedral K-rich micas close to the annite-phlogopite join with a general formula of $\text{K}(\text{Fe}, \text{Mg})_3(\text{Si}, \text{Al})_4\text{O}_{10}(\text{OH})_2$ accommodate a large number of different cations into their octahedral and tetrahedral sites. Understanding the complex crystal chemistry of these naturally occurring micas with multiple and complex cationic and anionic substitutions is difficult. In several studies, smooth systematic changes of physical and structural parameters (lattice parameters, mean bond lengths, ^{57}Fe hyperfine parameters) were shown to occur as a function of changing octahedral composition in “simplified” synthetic (pseudo)binary solid-solution series (e.g., Hazen and Wones 1972; Hewitt and Wones 1975; Redhammer et al. 1993; 1995; Rancourt et al. 1994; Rancourt et al. 1996; Redhammer 1998; 2001). The samples used in these studies were fine-grained powders, and because of this any structural information is limited to data extracted from Rietveld refinements of X-ray powder data (Redhammer et al. 2000). More complete information,

including accurate bond angles and polyhedral distortion parameters, is needed to obtain a comprehensive understanding of structural changes and deviations from ideal geometry as a consequence of changes in the chemical composition. Further, structural data of (near) end-member compositions are important input data for the calculation of the electric-field gradient and the ^{57}Fe hyperfine parameter. These data are important in understanding the physics of quadrupole splitting distributions observed in the Mössbauer spectra of micas (e.g., Rancourt et al. 1994; Redhammer 1998; Redhammer et al. 2000 and references therein).

We have performed single-crystal X-ray diffraction studies on synthetic trioctahedral micas with different octahedral compositions, ranging from Ni-phlogopite¹ $\text{KNi}_3\text{Si}_3\text{AlO}_{10}(\text{OH})_2$ to Mg-rich micas of the annite $\text{KFe}_3\text{Si}_3\text{AlO}_{10}(\text{OH})_2$ -phlogopite $\text{KMg}_3\text{Si}_3\text{AlO}_{10}(\text{OH})_2$ binary join (ferroann phlogopite). In addition, three naturally occurring Fe^{2+} , Al^{3+} -rich samples close to the annite-siderophyllite join (ann-sid) and one synthetic near end-member siderophyllite sample $\text{KFe}_2\text{AlSi}_2\text{Al}_2\text{O}_{10}(\text{OH})_2$ were

* Corresponding address: Neuhofen i.I. 224/TOP 1, A-4910 Ried im Innkreis, Austria. E-mail: guenther.redhammer@aon.at

¹Mineral names used here refer to synthetic products as well.

investigated. The major goals of this study were (1) to correlate structural changes with mean octahedral ionic radii (Shannon 1970), (2) to correlate deviations from ideal geometry (distortion) of polyhedra with chemical composition and mean M-O bond lengths, and (3) to provide structural data of synthetic end-member (and natural near end-member) compositions for subsequent theoretical electric-field gradient calculations, particularly for annite, siderophyllite, and phlogopite compositions.

Recently, a larger number of structural investigations have been done by single-crystal methods on natural (especially Brigatti and Davoli 1990; Brigatti et al. 1991; Brigatti and Poppi 1993; Brigatti et al. 1996a, b; Brigatti et al. 1998; Brigatti et al. 2000a, 2000b; Brigatti et al. 2001) and synthetic (McCauley et al. 1973; Comodi et al. 1999) micas close to the annite-phlogopite join. Concerning cationic ordering of Fe^{2+} , Mg^{2+} on the two non-equivalent M1 and M2 octahedral sites of natural trioctahedral 1M micas Brigatti and Davoli (1991) and Brigatti et al. (2000a) noted the possibility of a slight preference of Fe^{2+} for the M1 site. Based on geometric and chemical features, Cruciani and Zanazzi (1994) noted a preferential partitioning of high-charge cations (Ti^{4+} , Al^{3+} , Cr^{3+} , and Fe^{3+}) in the M2 site. Very recently, Brigatti et al. (2001) also found preferences of Ti^{4+} for the M2 site in Ti^{4+} rich trioctahedral 1M micas. For Al^{3+} clear evidence for cationic ordering was found very recently. In Fe^{2+} , Al^{3+} -rich micas close to the annite-siderophyllite binary, Brigatti et al. (2000a) note a preference of octahedral Al^{3+} for the M2 site. The same was found independently by Redhammer et al. (2000) from Rietveld refinements. Previously, Guggenheim and Eggleton (1987) suggested a crystal chemical reason why $^{16}\text{Al}^{3+}$ would prefer the M2 over the M1 site in the micas.

EXPERIMENTAL METHODS

Syntheses of mica single crystals (Table 1) were performed in a high-pressure/high-temperature piston-cylinder apparatus at temperatures of 1200–1250 °C and pressures of 2.5 GPa for

at least 48 hours. About 10–20 mg of the starting material, together with excess of water, was placed in a small platinum capsule (2–4 mm in length, inner diameter 1.5 mm) that was welded tight. After completing the experiment, the integrity of the capsule was tested by weighting the capsule, opening it, drying at 80 °C, and weighting it again. Starting materials were prepared either by the gelling method as described by Hamilton and Henderson (1968) (mixtures A20, A40, A60, and A80, which were previously prepared by Redhammer et al. 1995) or by mixing K_2CO_3 and metal oxides (NiO , MgO , CoO , Fe_2O_3 , SiO_2 , Al_2O_3) in the stoichiometry of the desired composition (cf. Redhammer 2001).

Electron-microprobe analysis (JEOL JXA 8600, acceleration voltage 15 kV, beam current 30 nA, beam focused to about 3 μm spot size) was used to determine the chemical composition of the mica products. Minerals were used as standards. Because of the small amounts of sample product available, standard epoxy mounts were not made and H_2O content and Mössbauer data could not be determined. Instead, several mica flakes were fixed with carbon tape onto a glass slide, and were coated with carbon and then analyzed. This procedure gives consistent results, although the weight percent sums are lower than expected. Calculated mineral formula in Table 2 are based on $\text{O}_{10}(\text{OH})_2$.

Single-crystal X-ray diffraction data sets were measured with an imaging-plate diffractometer system (Stoe-IPDS, $\text{MoK}\alpha$ radiation, pyrolytic graphite monochromator). Intensity data were collected to $56.5^\circ 2\theta$ within a ϕ -range of 0–229.5°, and the ϕ increment was 1.5°/image. This procedure produces 153 images per measurement. Except for samples no. NiPhl, no. Phl, no. CoAn and no. Ann, all lattice parameters were determined from the single-crystal X-ray diffraction measurements (about 1500 measured reflections). For the former samples, sufficient amounts and purity were obtained for powder X-ray diffraction (Siemens D500, $\text{CuK}\alpha$ radiation, 10–90° 2θ graphite monochromator, silicon used as an internal standard). For these samples, the lattice parameters of the powder

TABLE 1. Experimental conditions and results of mica synthesis

Sample*	Starting material composition	T†	P†	t†	Products‡
NiPhl	$\text{KNi}_3\text{Si}_3\text{AlO}_{10}(\text{OH})_2$	1250	2.5	67	mi, (ol)
Phl	$\text{KMg}_3\text{Si}_3\text{AlO}_{10}(\text{OH})_2$	1250	2.5	61	mi
GaPhl	$\text{KMg}_3\text{Si}_3\text{GaO}_{10}(\text{OH})_2$	1250	2.5	61	mi
CoAn	$\text{KCo}_3\text{Si}_3\text{AlO}_{10}(\text{OH})_2$	1250	2.5	72	mi, (ol)
A20	$\text{K}(\text{Mg}_{2.4}\text{Fe}_{0.6})\text{Si}_3\text{AlO}_{10}(\text{OH})_2$	1250	2.5	59	mi, (mt, sa), gl
A40	$\text{K}(\text{Mg}_{1.8}\text{Fe}_{1.2})\text{Si}_3\text{AlO}_{10}(\text{OH})_2$	1200	2.5	66	mi, (mt, sa), gl
A60	$\text{K}(\text{Mg}_{1.2}\text{Fe}_{1.8})\text{Si}_3\text{AlO}_{10}(\text{OH})_2$	1200	2.5	63	mi, mt, sa, gl
A80	$\text{K}(\text{Mg}_{0.6}\text{Fe}_{2.4})\text{Si}_3\text{AlO}_{10}(\text{OH})_2$	1200	2.5	60	mi, mt, sa, gl
A100	$\text{KFe}_3\text{Si}_3\text{AlO}_{10}(\text{OH})_2$	1300	2.5	51	gl
		1200	2.5	47	gl
		1100	2.5	63	gl
		1000	2.6	39	gl
		950	2.5	49	mi (powder)
Mga1.2	$\text{K}(\text{Mg}_{1.2}\text{Fe}_{1.8})\text{Si}_3\text{AlO}_{10}(\text{OH})_2$	1200	2.5	53	mi, mt, sa, gl
Mga1.6	$\text{K}(\text{Mg}_{1.6}\text{Fe}_{1.4})\text{Si}_3\text{AlO}_{10}(\text{OH})_2$	1200	2.5	70	mi, (mt, sa), gl
CoNi1.8	$\text{K}(\text{Co}_{1.8}\text{Ni}_{1.2})\text{Si}_3\text{AlO}_{10}(\text{OH})_2$	1250	2.5	53	mi, ol
CoNi1.2	$\text{K}(\text{Co}_{1.2}\text{Ni}_{1.8})\text{Si}_3\text{AlO}_{10}(\text{OH})_2$	1250	2.5	73	mi, (ol)
Sd87	$\text{K}(\text{Fe}_{2.13}\text{Al}_{0.87})(\text{Al}_{1.87}\text{Si}_{2.13})\text{O}_{10}(\text{OH})_2$	700	0.2	631	mi

* In the following Tables, individual crystals coming out from a specific sample are denoted by ...#, e.g., crystal A20#2 is the 2nd crystal measured from experiment A20.

† T = temperature (in DEG), P = pressure (in GPa), t = experiment duration (in h).

‡ mi = mica, mt = magnetite, sa = sanidine, gl = glass, ol = olivine; mineral abbreviations in parentheses are below 5 vol% of experimental product (estimated from optical microscopy).

TABLE 2a. Chemical composition (wt %) and structural formula [apfu, based on O₁₀(OH)₂] of synthetic micas as determined by electron microprobe analysis

Sample	NiPhl	Coni1.2	CoNi1.8	CoAn	Phl	A20	A40	A60	A80_a	A80_b	A80_c	Mga1.2	Mga1.6	Sd87
n	25	25	23	25	25	15	17	14	7	5	5	20	20	20
K ₂ O	9.1(1)	8.5(1)	9.1(1)	9.1(2)	10.9(1)	10.6(1)	10.5(1)	10.5(1)	10.7(1)	10.6(2)	10.5(2)	9.9(2)	10.6(1)	9.3(1)
NiO	43.3(2)	26.5(3)	18.8(4)	—	—	—	—	—	—	—	—	—	—	—
CoO	—	15.6(4)	23.9(5)	41.9(4)	—	—	—	—	—	—	—	—	—	—
MgO	—	—	—	—	28.3(3)	24.5(3)	22.0(2)	21.1(6)	21.8(3)	20.1(3)	17.4(3)	19.1(3)	22.6(2)	—
FeO	—	—	—	—	—	5.4(1)	8.5(3)	9.0(1)	9.1(2)	10.8(2)	14.0(3)	12.6(4)	8.0(2)	31.0(2)
SiO ₂	34.1(3)	32.9(5)	33.4(4)	33.2(4)	41.3(2)	39.7(4)	39.5(4)	37.7(5)	40.1(4)	39.3(3)	37.8(3)	38.5(4)	39.5(2)	27.1(2)
Al ₂ O ₃	11.1(2)	10.6(3)	11.1(2)	11.2(4)	13.5(2)	13.0(2)	12.1(2)	12.0(1)	12.9(1)	12.5(1)	11.2(1)	11.4(5)	12.2(2)	25.3(2)
Sum	97.7(3)	94.2(5)	96.3(5)	95.4(4)	94.0(4)	93.0(5)	92.5(8)	90.2(7)	94.6(4)	93.3(5)	90.8(4)	91.5(5)	92.8(4)	92.6(3)
K ⁺	1.00(1)	0.96(2)	1.00(1)	1.02(2)	0.99(1)	0.99(1)	1.00(1)	1.02(2)	1.00(1)	1.02(1)	1.05(1)	0.97(1)	1.00(1)	1.00(1)
Ni ²⁺	2.98(3)	1.90(4)	1.32(3)	—	—	—	—	—	—	—	—	—	—	—
Co ²⁺	—	1.11(3)	1.67(4)	2.94(4)	—	—	—	—	—	—	—	—	—	—
Mg ²⁺	—	—	—	—	2.98(3)	2.68(4)	2.45(3)	2.35(6)	2.39(2)	2.25(2)	2.04(2)	2.19(3)	2.51(2)	—
Fe ²⁺	—	—	—	—	—	0.33(1)	0.53(3)	0.68(1)	0.56(2)	0.68(2)	0.92(2)	0.82(3)	0.50(1)	2.18(2)
Al ³⁺	0.04	0.02	0.04	0.06	0.03	0.03	0.03	0.01	0.05	0.06	0.02	0.01	0.01	0.79(1)
Sum Oct.	3.02	3.03	3.03	3.00	3.01	3.04	3.01	3.04	3.00	2.99	2.98	3.02	3.02	2.97
Al ³⁺	1.08(1)	1.08(3)	1.09(2)	1.09(4)	1.08(1)	1.09(1)	1.04(1)	1.09(2)	1.06(2)	1.05(2)	1.02(2)	1.03(4)	1.06(2)	1.72(2)
Si ⁴⁺	2.92(2)	2.92(2)	2.91(3)	2.91(2)	2.92(2)	2.91(2)	2.96(2)	2.91(2)	2.94(1)	2.95(2)	2.98(3)	2.97(4)	2.94(1)	2.28(1)
Sum Tet.	4.00	4.00	4.00	4.00	4.00	4.00	4.00	4.00	4.00	4.00	4.00	4.00	4.00	4.00

Note: n = number of analyses; numbers in parentheses are the estimated standard deviations and refer to the last digit.

TABLE 2b. Composition [based on O_{12-(x+y+z)}(OH)_xF_yCl_z] of the three natural Fe²⁺-, Al³⁺-rich micas investigated by single-crystal X-ray structure refinement in the present study

Sample	Ann*	Sdp*	G-117†
K ⁺	0.937	0.892	0.997
Na ⁺	0.075	0.040	0.010
Σ Int.	1.012	0.932	1.007
Mg ²⁺	0.074	0.054	0.109
Fe ²⁺	2.250	1.949	1.903
Fe ³⁺	0.284	0.096	0.476
Al ³⁺	0.001	0.657	0.272
Mn ²⁺	0.175	0.119	0.035
Ti ⁴⁺	0.079	0.017	0.036
Cr ³⁺	—	0.003	—
Σ Oct.	2.862	2.894	2.831
Al ³⁺	0.980	1.436	1.450
Si ⁴⁺	2.826	2.492	2.550
Fe ³⁺	0.194	0.072	—
Σ Tet.	4	4	4
OH ⁻	1.847	1.872	1.900
F ⁻	0.148	0.106	0.033
Cl ⁻	0.005	0.023	0.003

Note: data are from electron microprobe analysis, Fe²⁺/Fe³⁺ ratio as determined by Mössbauer spectroscopy.

* Lalonde et al. (1996), data from Table 1, Ann = annite, Sdp = siderophyllite.

† Litchfield/Barker biotite G-117, analysis courtesy of M.D. Dyar. Fe²⁺ and Fe³⁺ values determined by Mössbauer spectroscopy.

X-ray diffraction experiments were used in the structure refinement.

Only crystals of sufficient size (at least 0.05 × 0.05 × 0.01 mm), which gave sharp reflections and showed well-defined periodicity along c*, were used for intensity data collection. About 25 crystals were examined for each composition because many crystals showed significant numbers of stacking faults along c* direction. All crystals examined and subsequently investigated were 1M polytypes, therefore all refinements were performed in space group C2/m (12). The programs X-SHAPE

(Stoe and Cie 1996) and SHELXL (Sheldrick 1997) were used for absorption correction and structure refinement, respectively. The atomic positions of Hazen and Burnham (1973) were used as initial values for the structure refinements. The position of the hydrogen atom was obtained from difference-Fourier maps and each was close to the position determined by Joswig (1972) for phlogopite, i.e., x = 0.098(2), y = 1/2, z = 0.3007(8).

RESULTS

Synthesis

Synthesis of mica single crystals suitable for single-crystal X-ray diffraction is not straightforward. In more than two-thirds of the experiments, the platinum capsules leaked. In these cases, only the anhydrous decomposition products were found and the samples were rejected. Table 1 summarizes the conditions and products of successful experiments. Single-phase products here are rare. Only the products of the phlogopite composition did not show additional phases. Traces of Co-olivine (Co₂SiO₄) and Ni-olivine (Ni₂SiO₄) single crystals were found along with the micas (less than 0.2 × 0.2 × 0.03 mm in size) in the products of no. CoAn and no. NiPhl, respectively. Sample no. CoNi1.8 contained greater amounts of olivine with composition Co_{1.67}Ni_{0.32}Si_{1.00}O₄ (from EMP analysis). Individual mica crystals of this sample of the KNi₃Si₃AlO₁₀(OH)₂-KCo₃Si₃AlO₁₀(OH)₂ solid solution series were smaller than those of end-member compositions. The same applies to no. CoNi1.2. However, for this composition, no suitable single crystal was found. Synthesis of Fe-bearing micas was more difficult. For experiments with Fe-bearing starting materials, no pure phases were obtained, except no. A20. For other experiments with Fe-bearing starting materials, products contained significant amounts of sanidine, magnetite, traces of quartz, and variable amounts of brown glass. These phases made up <50% of the total product. Sample no. A80 contained two micas with slight differences in color, and corresponding small differences in compositions based EMP analyses. In general, the Fe-bearing

micas are small in size and brown to black in color.

Attempts to grow single crystals from gels or from oxide mixtures of annite starting compositions failed. Synthesis performed between 1300 °C and 1050 °C showed green to black homogenous glass, if the completed experiment still contained water. In an experiment run at 950 °C and 2.5 GPa, the stable product was annite but the grain size remained <0.005 mm.

Sample no. Sd87 involved an experiment (700 °C, 0.2 GPa, cold-sealed pressure vessels) to synthesize large amounts of an Al³⁺-rich mica on one side of a 5 cm long gold tube. Crystals were pale blue-green and appeared as large (0.02–0.03 mm) but thin plates (0.003 mm) in the matrix of fine-grained micas of similar composition. Details on hydrothermal synthesis of mica on the annite-siderophyllite join are given in Redhammer et al. (2000).

Mineral chemistry

Electron microprobe analyses of the synthetic samples are given in Table 2a and Table 2b shows the composition of the three natural micas. The synthetic micas are slightly depleted in Si⁴⁺ and correspondingly enriched in tetrahedral Al³⁺. Note that, in general, the aluminum content seems to be slightly overestimated, as indicated by excess populations of octahedral sites, after Al³⁺ is assigned to the tetrahedral sites to obtain 4 cations per formula unit. The small amount (<0.05 apfu) of octahedrally coordinated Al³⁺ (Table 2a) may not be real, except for samples no. A80 and no. Sd87 where the Al³⁺ excess is obvious. The EMP analysis shows that, even if starting with iron-rich compositions (e.g., no. A80), the iron content does not exceed ≈0.80 Fe atoms per formula unit (apfu). Mica products of the annite-phlogopite series moved away from their nominal composition and are more Mg-rich than the starting composition. Currently we have no good explanation for these findings.

For compositions between Ni-phlogopite and Co-phlogopite, the Co²⁺ to Ni²⁺ ratio of the mica products is close to the starting composition. The synthetic Al³⁺-rich annite no. Sd87 contains 0.79 apfu of octahedrally coordinated Al³⁺, which is close to the limit of Al³⁺ solubility in octahedral sites at 700 °C as determined by Redhammer et al. (2000). Thus, no. Sd87 represents a mica with a composition as close as possible to the ideal composition of siderophyllite.

The three natural samples correspond to Fe²⁺, Al³⁺-rich trioctahedral micas close to the annite-siderophyllite join. The natural annite (no. ann) is closer to the ideal composition of annite than the one investigated by Hazen and Burnham (1973). It contains very low amounts of Al and Mg but considerable concentrations of Mn²⁺ (Table 2b). Sample no. G-117 is intermediate between annite and siderophyllite composition, and sample no. Sdp is close to the ideal siderophyllite composition. Sample no. Sdp contains low concentrations of Mg²⁺, and plots on the annite-siderophyllite binary join.

Single-crystal X-ray diffraction

Details on data collection, results of structure refinement, lattice parameters, fractional atomic positional coordinates, and equivalent isotropic displacement parameters of synthetic and natural mica crystals are given in Tables 3a and 3b respectively.

Anisotropic atomic displacement parameters are given in Table 4a and 4b. Tables 5a and 5b contain selected bond lengths, bond angles, and distortion parameters for the samples given in Tables 3. The atomic labeling is the same as in Hazen and Burnham (1973). Refinements converged to R_1 values in the range 0.020–0.058. Difference electron density (DED) maps were calculated to locate the hydrogen atom. The standard deviation σ of the DED-map was in the range 0.11–0.18 e/Å³ for all measurement. One to five DED-peaks were above background (3σ); however, based on bond length considerations, only one of them represents a reasonable hydrogen position. In all refinements, this residual electron density was found close to the O4 O atom with heights of 0.85 to 0.98 e/Å³ and atomic coordinates close to those given by Joswig (1972) for hydrogen in phlogopite. Including this DED-peak in the refinement slightly improves the R factors, e.g., wR_2 was lowered by ≈1.2–1.8%. Thus this electron density was assigned to the hydrogen atom and its atomic coordinates were freely refined in the final stage of the structure refinement, whereas the isotropic atomic displacement parameter was fixed to a U_{eq} value of 0.03 ($B_{eq} = 2.35 \text{ \AA}^2$). The fractional atomic coordinates stayed in place during refinement. The resulting O4-H distances range from 0.73 to 1.13 Å and are acceptable for O-H distances in micas. For more details on hydrogen position assignment in micas refer to Nelson and Guggenheim (1993).

DISCUSSION

Atomic displacement parameters

All the single-crystal structure refinements were done with anisotropic atomic displacement parameters. The cations are nearly isotropic, whereas the O atoms are more anisotropic, especially the O1 and O2 O atoms, which form the base of the Si,Al tetrahedra. Based on the equivalent isotropic atomic displacement parameters (Tables 3a and 3b) the tetrahedral site shows the smallest thermal vibration, along with the two M sites. The interlayer cation has the highest thermal vibration and shows an anisotropic elongation along the **a** and **b** axis within the (001) plane. The O1 and O2 O atoms, which coordinate to the tetrahedral and the interlayer cation, show larger thermal vibrations than the O3 and O4 O atoms, which coordinate to the M site cations. These observations are in accordance with the strengths of the bonds affecting each site. The larger atomic displacement parameters of the O1 and O2 O atoms probably are related to the tetrahedral size difference owing to Si and Al substitutions. The O1 and O2 atoms are also more susceptible to displacements than the O3 O atom. The latter is bonded to the octahedral as well as to the tetrahedral cations, whereas the O1 and O2 O atoms are bonded to the tetrahedral and the interlayer cations, and therefore are not bonded as strongly as the O3 O atom.

The octahedral sheet

Figure 1 displays the variation of the mean M1-O and mean M2-O distances vs. averaged octahedral cation ionic radius (Shannon 1970) of the M sites. Except for the Fe²⁺-, Al³⁺-rich micas studies by Brigatti et al. (2000a, b) no evident relations of mean M-O with mean octahedral cation radius are found in

the literature because of different geological settings and the complex chemistry and multiple cationic substitutions of these micas. The mean M1-O bond lengths vs. octahedral cation ionic radii (Fig. 1a) of micas with tetrahedral site compositions near Si_3Al define—as would be expected—a nearly linear relationship with decreasing of mean M1-O when ferrous iron is substituted by smaller cations (Co^{2+} , Mg^{2+} , Ni^{2+}). The mean M1-O bond lengths vs. octahedral cation ionic radii of the siderophyllite-rich Fe^{2+} , Al^{3+} micas however do not plot onto this line, but define, along with the data of Brigatti et al. (2000a, b) a separate trend with smaller slope. This behavior is explained by the preference of Al^{3+} for the M2 position (Brigatti et al. 2000a; Redhammer et al. 2000). M-site occupation refinements of the Fe^{2+} -, Al^{3+} -rich samples support this finding. For the synthetic siderophyllite sample no. Sd87, 0.204 apfu Al^{3+} was found at the M1 site, whereas 0.618 apfu Al^{3+} occupy the M2 sites. The amount of octahedral Al^{3+} found by structure refinement

($\text{Al}^{3+} = 0.822$ apfu) and EMP analysis ($\text{Al}^{3+} = 0.79$ apfu) is in good agreement. The natural sample no. Sdp behaves accordingly. Here, the refined cationic distribution is $^{\text{M1}}[\text{Fe}_{0.723}\text{Al}_{0.180}]^{\text{M2}}[\text{Fe}_{1.447}\text{Al}_{0.519}]$ and there is significantly lower Al^{3+} at the M1 site as compared to the M2 site. For the latter refinement, Mg^{2+} was treated as Al^{3+} and Mn^{2+} as Fe^{2+} . Table 6a summarizes octahedral-site occupation as determined by structure refinement. In Figure 1a, most of the mean M1-O vs. octahedral cation ionic radii data obtained from the literature plot in a field defined by the regression curves through the data for the Fe^{2+} -, Al^{3+} -rich micas and the micas with Si_3Al tetrahedral composition investigated in this study. Most of the natural trioctahedral micas contain significant amounts of octahedral Al^{3+} and this preferentially occupies the M2 sites.

The mean M2-O bond lengths of micas with Si_3Al tetrahedral composition fall onto one common nearly linear trend (Fig. 1b). The mean M2-O bond lengths of the three natural Fe^{2+} -,

TABLE 3a. Details on structure refinement, lattice parameters, fractional atomic coordinates, and equivalent atomic displacement parameters for selected synthetic trioctahedral 1M micas

	NiPhl#6	Phl#2	CoAn#2	Coni1.8#2	A20#2	A20#4
N_{observed}	2228	2230	2364	2132	2412	2421
N_{unique}	628	568	620	566	616	576
R_{int} (%)	5.80	2.06	4.00	3.27	4.47	5.83
$R_{\text{int}} > 4\sigma$ (%)	3.21	2.09	3.26	3.41	4.31	2.71
R_{all} (%)	7.54	2.87	3.82	4.66	5.58	5.33
$wR_{\text{int}} > 4\sigma$ (%)	8.34	6.04	7.15	7.64	10.63	5.80
wR_{all} (%)	8.97	10.2	8.78	9.61	13.25	6.45
GOF*	0.914	1.871	1.114	1.313	1.027	0.976
a (Å)	5.3023(20)	5.3158(24)	5.3380(19)	5.3225(21)	5.3257(28)	5.3245(22)
b (Å)	9.1804(36)	9.2036(34)	9.2465(38)	9.2195(32)	9.2254(31)	9.2245(44)
c (Å)	10.2911(38)	10.3100(57)	10.3410(38)	10.3125(48)	10.3070(61)	10.3050(36)
β (°)	99.921(44)	99.891(59)	99.977(43)	99.949(51)	99.926(66)	99.927(45)
V (Å ³)	493.45	496.91	502.69	498.43	498.82	498.56
S.G.	$C2/m$	$C2/m$	$C2/m$	$C2/m$	$C2/m$	$C2/m$
T (x)	0.57689(23)	0.57651(9)	0.57610(18)	0.57637(21)	0.57616(13)	0.57621(12)
T (y)	0.16663(16)	0.16674(4)	0.16668(8)	0.16674(7)	0.16672(7)	0.16690(7)
T (z)	0.23009(12)	0.22952(4)	0.22778(8)	0.22848(9)	0.22873(8)	0.22879(8)
T B_{eq} (Å ²)	0.55(2)	0.63(3)	0.83(3)	0.84(2)	0.86(2)	0.65(2)
M1 B_{eq} (Å ²)	0.66(3)	0.64	0.91(3)	0.69(2)	0.79(4)	0.57(5)
M2 (y)	0.83198(11)	0.83171(7)	0.83147(6)	0.83190(5)	0.83241(11)	0.83248(12)
M2 B_{eq} (Å ²)	0.66(3)	0.63	0.95(6)	0.70(1)	0.75(3)	0.57(4)
K B_{eq} (Å ²)	2.77(5)	3.54	2.87(4)	2.62(4)	2.91(3)	2.62(3)
O1 (x)	0.83411(73)	0.83048(25)	0.82584(32)	0.82794(52)	0.83088(37)	0.82982(34)
O1 (y)	0.22589(47)	0.22662(13)	0.23063(22)	0.22891(28)	0.22634(25)	0.22710(22)
O1 (z)	0.17263(37)	0.17165(10)	0.17050(23)	0.17079(24)	0.17177(20)	0.17142(21)
O1 B_{eq} (Å ²)	1.43(5)	1.40	1.61	1.68(5)	1.80(4)	1.41(4)
O2 (x)	0.50706(56)	0.50995(35)	0.51819(51)	0.51410(34)	0.50953(57)	0.51106(51)
O2 (y)	0.17330(48)	0.17174(14)	0.17061(28)	0.17080(34)	0.17173(28)	0.17167(31)
O2 B_{eq} (Å ²)	1.48(6)	1.38(5)	1.62(5)	1.69(7)	1.87(5)	1.46(6)
O3 (x)	0.63163(62)	0.63068(21)	0.62987(32)	0.63136(51)	0.62998(33)	0.63084(30)
O3 (y)	0.16634(41)	0.16673(10)	0.16676(17)	0.16663(20)	0.16682(18)	0.16673(19)
O3 (z)	0.39342(31)	0.39172(14)	0.39048(19)	0.39129(20)	0.39159(19)	0.39157(19)
O3 B_{eq} (Å ²)	0.71(3)	0.76(4)	0.98(3)	0.82(4)	0.85(3)	0.74(3)
O4 (x)	0.13367(45)	0.13248(30)	0.13211(42)	0.13362(70)	0.13254(45)	0.13284(51)
O4 (y)	0.39940(55)	0.39880(14)	0.39758(28)	0.39809(29)	0.39861(25)	0.39918(29)
O4 B_{eq} (Å ²)	0.76(2)	0.83(3)	1.06(2)	0.87(2)	0.95(3)	0.97(5)
H (x)	0.103(11)	0.111(8)	0.116(10)	0.111(9)	0.130(9)	0.093(8)
H (z)	0.309(5)	0.318(4)	0.303(9)	0.288(6)	0.313(5)	0.325(5)
H B_{eq} (Å ²)	2.35	2.35	2.35	2.35	2.35	2.35

Note: Special positions for M1 = 0, $1/2$, $1/2$; M2 = 0, y , $1/2$; K = 0, 0, 0; O2 = x , 0, z ; O4 = x , 0, z and H = x , 0, z .

* GOF = Goodness of Fit parameter: $\text{GOF} = \sqrt{\frac{\sum w(F_o^2 - F_c^2)^2}{n-p}}$ where n is the number of reflections and p is the number of parameters refined.

Al³⁺-rich micas and the synthetic samples of the annite-siderophyllite series (Redhammer et al. 2000) plot on a common trend. For the literature data, the spread of data points is much smaller for the mean M2-O than for the mean M1-O bond lengths.

For each mica with a Si₃Al tetrahedral composition, the average M1-O vs. average M2-O bond lengths are nearly identical in size to within one estimated standard deviation (Table 5). Only for annite (Anno. 1, Table 5b), is there a difference of 0.005(2) Å between mean M1-O and mean M2-O. These results are in contradiction to other studies of natural samples. For natural (fluoro)phlogopite, Hazen and Burnham (1973) also found similar mean M1-O and mean M2-O bond lengths, but for natural annite mean M1-O and mean M2-O differ by 0.02 Å. Most samples investigated by Brigatti and coworkers also show large differences between mean M1-O and mean M2-O of 0.01 to 0.025 Å. Besides annite, differences between mean

M1-O and mean M2-O ($\Delta <M-O>$) are evident only for the Fe²⁺-, Al³⁺-rich samples close to the annite-siderophyllite join in the present study. We assume that in most of these samples from the literature, this $\Delta <M-O>$ value is related to octahedrally coordinated Al³⁺ and the tendency for Al³⁺ enrichment at M2. This is supported by recent findings of Brigatti et al. (2001) who found equivalent mean bond distances for M1 and M2 sites in micas with low to very low Al³⁺ contents (phlogopite, ferroan phlogopite, and ferroan tetra-ferri-phlogopite).

Divalent cationic substitution not only reduces the M1-O and M2-O bond lengths but also the thickness of the octahedral sheet. The thickness decreases almost linearly from ≈ 2.24 Å in annite (no. Ann) to about 2.12 Å in "Ni-phlogopite" (no. NiPhl) as a function of the size of the octahedral cation. Samples along the annite-siderophyllite join (no. G-117, no. Sdp, no. Sd87) exhibit a slightly more pronounced decrease of octahedral sheet thickness with decreasing mean octahedral ionic radius (Table 4).

TABLE 3a. — Extended

A40#7	A60#2	Mga1.2#1	Mga1.6#4	Sd87#4	GaPhl#1
2236	2433	2269	2397	2207	2445
633	628	629	618	642	617
4.36	3.38	6.01	3.35	3.59	2.75
2.46	2.97	4.56	1.99	2.57	2.13
5.55	4.25	6.62	3.00	3.72	2.95
6.46	7.49	5.27	5.12	6.13	5.59
7.83	8.62	8.45	5.12	6.13	6.30
0.953	1.101	1.284	0.975	1.009	1.071
5.3295(23)	5.3384(22)	5.3409(21)	5.3257(16)	5.3649(23)	5.3214(26)
9.2309(35)	9.2465(28)	9.2536(24)	9.2241(35)	9.2892(28)	9.2140(27)
10.3074(53)	10.3061(38)	10.3087(37)	10.3056(27)	10.2698(45)	10.3896(34)
99.944(56)	99.951(46)	99.962(43)	99.932(33)	100.242(51)	99.717(41)
499.47	501.07	501.80	498.67	503.65	502.11
<i>C2/m</i>	<i>C2/m</i>	<i>C2/m</i>	<i>C2/m</i>	<i>C2/m</i>	<i>C2/m</i>
0.57604(14)	0.57557(12)	0.57634(21)	0.57576(8)	0.57595(12)	0.57612(7)
0.16684(7)	0.16681(6)	0.16674(11)	0.16683(4)	0.16683(6)	0.16673(4)
0.22793(8)	0.22750(6)	0.22776(13)	0.22793(5)	0.22658(6)	0.22866(4)
1.16(3)	0.58(2)	1.31(3)	0.58(1)	0.58(2)	0.53
1.07(4)	0.70(4)	1.26(6)	0.56(3)	0.50(2)	0.34
0.83302(12)	0.83449(9)	0.83387(16)	0.83388(7)	0.83139(5)	0.83269(9)
1.07(3)	0.63(3)	1.23(4)	0.56(2)	0.49(2)	0.35
3.44(4)	2.56(3)	3.67(6)	2.59(2)	2.14(4)	2.14
0.82811(42)	0.82792(34)	0.82827(41)	0.82878(24)	0.83672(31)	0.83456(31)
0.22858(25)	0.22795(22)	0.22845(36)	0.22745(15)	0.22050(20)	0.22253(19)
0.17137(20)	0.17027(16)	0.17024(33)	0.17055(14)	0.17265(18)	0.17097(17)
2.36(4)	1.50(3)	2.28(6)	1.50(2)	1.52(3)	1.70
0.51447(51)	0.51183(52)	0.51402(48)	0.51118(36)	0.49960(48)	0.50088(47)
0.17135(32)	0.17102(24)	0.17123(32)	0.17082(19)	0.17334(25)	0.17107(24)
2.34(6)	1.56(5)	2.36(8)	1.52(4)	1.51(5)	1.73
0.63030(35)	0.63012(31)	0.63027(34)	0.63032(21)	0.63333(35)	0.63028(26)
0.16747(18)	0.16712(17)	0.16727(29)	0.16706(12)	0.16776(17)	0.16729(13)
0.39006(19)	0.39127(17)	0.38943(28)	0.39130(13)	0.39449(17)	0.39206(15)
1.23(4)	0.71(3)	1.34(5)	0.73(2)	1.17(3)	1.73
0.13240(52)	0.13300(42)	0.13309(70)	0.13321(31)	0.12691(47)	0.13357(37)
0.39630(32)	0.39854(23)	0.39728(42)	0.39910(19)	0.39857(24)	0.39915(21)
1.39(5)	0.76(4)	1.64(6)	0.80(3)	1.39(4)	0.64
0.121(9)	0.116(8)	0.125(11)	0.113(6)	0.100(9)	0.105(10)
0.315(8)	0.296(4)	0.309(7)	0.328(4)	0.301(6)	0.325(5)
2.35	2.35	2.35	2.35	2.35	2.35

TABLE 3b. Details of structure refinement, lattice parameters, fractional atomic coordinates, and equivalent atomic displacement parameters for the three natural trioctahedral 1M micas

	Ann#1	G-117	Sdp#3
N_{observed}	2498	2538	2014
N_{unique}	645	640	608
R_{int} (%)	4.62	2.87	4.93
$R_i > 4\sigma$ (%)	2.39	3.45	2.75
R_i all (%)	4.03	4.19	3.23
$wR_2 > 4\sigma$ (%)	5.18	9.52	6.67
wR_2 all (%)	5.52	10.03	7.27
GOF	0.944	1.064	1.182
a (Å)	5.4059(21)	5.3741(14)	5.3710(13)
b (Å)	9.3639(27)	9.3083(19)	9.3020(29)
c (Å)	10.3235(41)	10.2829(29)	10.2560(25)
β (°)	100.200(46)	100.220(32)	100.250(28)
V (Å ³)	514.32	506.23	504.27
S.G.	$C2/m$	$C2/m$	$C2/m$
T (x)	0.57218(12)	0.57540(15)	0.57587(11)
T (y)	0.16660(6)	0.16681(7)	0.16692(5)
T (z)	0.22473(6)	0.22577(8)	0.22617(5)
T B_{eq} (Å ²)	0.85(2)	0.97(2)	1.07(1)
M1 B_{eq} (Å ²)	0.86(2)	0.82(2)	1.02(2)
M2 (y)	0.83209(5)	0.83199(6)	0.83133(4)
M2 B_{eq} (Å ²)	0.86(1)	0.83(2)	1.06(2)
K B_{eq} (Å ²)	3.12(5)	2.89(5)	2.82(3)
O1 (x)	0.80853(36)	0.82658(38)	0.82850(25)
O1 (y)	0.24357(21)	0.22975(25)	0.22801(17)
O1 (z)	0.16801(19)	0.16961(20)	0.17015(14)
O1 B_{eq} (Å ²)	2.31(4)	1.95(4)	1.93(3)
O2 (x)	0.53927(59)	0.51517(58)	0.51258(37)
O2 (z)	0.16774(28)	0.17068(28)	0.17127(18)
O2 B_{eq} (Å ²)	2.29(5)	1.85(4)	1.93(4)
O3 (x)	0.62887(31)	0.63165(42)	0.63295(29)
O3 (y)	0.16638(15)	0.16790(19)	0.16808(14)
O3 (z)	0.38846(17)	0.39203(20)	0.39273(15)
O3 B_{eq} (Å ²)	1.16(3)	1.42(4)	1.59(3)
O4 (x)	0.12753(46)	0.12709(54)	0.12562(37)
O4 (z)	0.39288(26)	0.39672(27)	0.39761(22)
O4 B_{eq} (Å ²)	1.31(4)	1.52(5)	1.86(4)
H (x)	0.108(9)	0.117(10)	0.100(8)
H (z)	0.314(7)	0.305(5)	0.324(6)
H B_{eq} (Å ²)	2.35	2.35	2.35

In the present study, we investigated a total of eight samples along the annite $\text{KFe}_3\text{Si}_3\text{AlO}_{10}(\text{OH})_2$ -phlogopite $\text{KMg}_3\text{Si}_3\text{AlO}_{10}(\text{OH})_2$ join and refined the cationic distribution of Mg and Fe between the M1 and M2 sites. Table 6b summarizes the results, which are shown graphically in Figure 2. The distribution found is very close to a random distribution of Fe and Mg. If the two data points at high Fe concentrations are excluded, the remaining points suggest a slight preference of Fe for the M1 site. However, this suggestion is not strongly supported by the data. Brigatti and Davoli (1990) and Brigatti et al. (2000a) suggested a slight preference of Fe^{2+} for the M1 site as well.

Variations of polyhedral distortion parameters as a function of varying chemical composition are useful for interpreting variations of ^{57}Fe hyperfine parameters in Mössbauer spectroscopy. Figure 3 shows the change of the octahedral flattening angle ψ (Donnay et al. 1964, formula as given in Hazen and Burnham 1973) with changing mean M-O bond lengths for the M1 and M2 sites, respectively. The angle is smallest in annite ($\psi = 58.2^\circ$ and 58.1° for M1 and M2, respectively) as compared to the other micas investigated here, but still is distinctly different from the ideal value of 54.73° for an undistorted isolated octahedron without flattening. The ψ value increases with

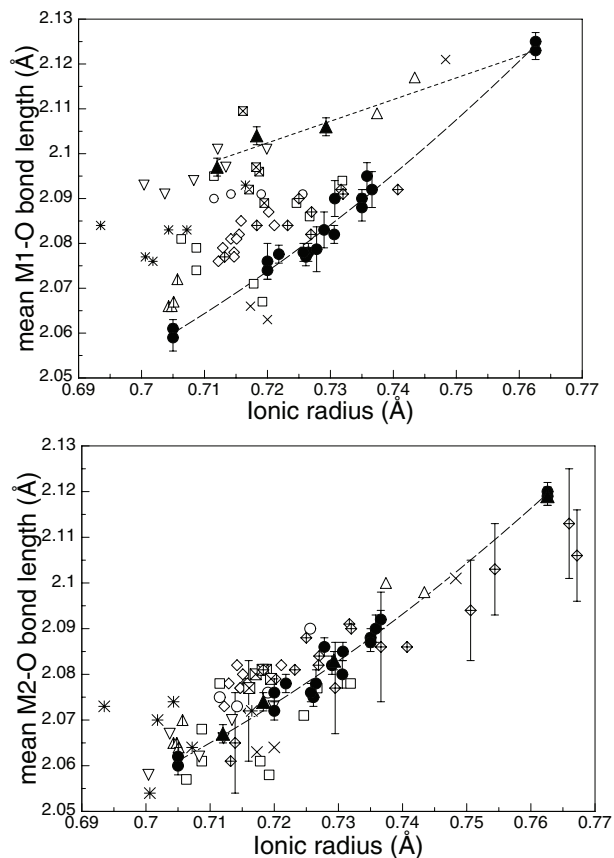


FIGURE 1. Variation of mean M1-O (a) and mean M2-O bond lengths (b) with mean octahedral ionic radii. Solid circles = data for synthetic trioctahedral 1M micas with Si_3Al tetrahedral composition of this study, solid triangles = data for Fe^{2+} -, Al^{3+} -rich 1M micas of this study; crosses = data from Hazen and Burnham (1973) and Joswig (1972); open diamonds = Brigatti et al. (1996a); open squares with cross inside = Brigatti and Davoli (1991); open squares = Brigatti et al. (1991); stars = Brigatti and Poppi (1993); open triangle pointing downward = Brigatti et al. (2000a); open circles = Brigatti et al. (1998); open triangle pointing upward = Brigatti et al. (2000b); open triangle with vertical line = Alietti et al. (1995); open diamonds with cross inside = Brigatti et al. (2001); diamonds with vertical line in Figure 1b = Redhammer et al. (2000a). Lines fitted to the data are guides to the eye.

decreasing mean M1-O and mean M2-O or with decreasing mean octahedral ionic radius. Incorporation of smaller cations into the octahedral sheet of annite increases the deviation from the ideal geometry of the octahedron and also of neighboring octahedra, which contain no smaller cations. Because of the shared edges, distortions of the different octahedra (M1 and M2) are linked. As for the variation of mean M1-O vs. mean octahedral cationic radius, there is large scatter of the octahedral flattening angles ψ_{M1} when plotted against the mean M1-O bond length. However, the data points lie within a field, which is limited by lines through the data for the micas with Si_3Al tetrahedral composition and those for samples close to the annite-siderophyllite join. As for bond lengths, the scatter in the literature data is related to the non-random distribution of Al^{3+} at the M1 and M2 sites. For the M2 site (Fig. 3b), the

TABLE 4a. Anisotropic atomic displacement factors U_i (\AA^2) for selected synthetic trioctahedral 1Mmicas

	NiPhl#6	Phl#2	CoAn#2	Coni1.8#2	A20#2	A20#4	A40#7	A60#2	Mga1.2#1	Mga1.6#4	Sd87#4	GaPhl#1	
T	U_{11}	0.0045	0.0067	0.0075	0.0073	0.0086	0.0056	0.0111	0.0056	0.0136	0.0063	0.0072	0.0066
	U_{22}	0.0068	0.0077	0.0074	0.0076	0.0095	0.0093	0.0091	0.0061	0.0119	0.0062	0.0069	0.0073
	U_{33}	0.0095	0.0094	0.0171	0.0094	0.0155	0.0099	0.0242	0.0103	0.0255	0.0094	0.0078	0.0065
	U_{23}	0.0002	-0.0001	0.0003	0.0001	0.0001	-0.0001	-0.0006	-0.0002	0.0005	-0.0001	-0.0004	-0.0001
	U_{13}	0.0012	0.0019	0.0033	0.0011	0.0046	0.0018	0.0044	0.0016	0.0065	0.0012	0.0011	0.0015
	U_{12}	0.0001	0.0000	0.0001	-0.0001	-0.0003	-0.0001	0.0001	-0.0003	0.0014	0.0001	-0.0004	0.0001
M1	U_{11}	0.0061	0.0059	0.0085	0.0067	0.0080	0.0046	0.0109	0.0076	0.0106	0.0055	0.0055	0.0033
	U_{22}	0.0064	0.0074	0.0071	0.0060	0.0075	0.0075	0.0117	0.0066	0.0112	0.0054	0.0046	0.0047
	U_{33}	0.0130	0.0112	0.0195	0.0133	0.0155	0.0102	0.0181	0.0129	0.0271	0.0105	0.0093	0.0053
	U_{13}	0.0032	0.0018	0.0033	0.0021	0.0051	0.0030	0.0025	0.0037	0.0067	0.0025	0.0019	0.0015
M2	U_{11}	0.0057	0.0061	0.0082	0.0069	0.0072	0.0033	0.0114	0.0050	0.0140	0.0048	0.0046	0.0031
	U_{22}	0.0069	0.0069	0.0076	0.0063	0.0077	0.0089	0.0115	0.0073	0.0099	0.0058	0.0049	0.0039
	U_{33}	0.0123	0.0114	0.0202	0.0132	0.0145	0.0096	0.0182	0.0113	0.0239	0.0105	0.0091	0.0062
	U_{13}	0.0015	0.0024	0.0034	0.0017	0.0040	0.0018	0.0034	0.0007	0.0059	0.0007	0.0011	0.0013
K	U_{11}	0.0391	0.0359	0.0186	0.0359	0.0387	0.0350	0.0458	0.0341	0.0490	0.0350	0.0305	0.0315
	U_{22}	0.0375	0.0377	0.0251	0.0354	0.0398	0.0385	0.0440	0.0339	0.0494	0.0354	0.0298	0.0325
	U_{33}	0.0279	0.0224	0.0215	0.0280	0.0328	0.0260	0.0409	0.0289	0.041	0.0275	0.0204	0.0170
	U_{13}	0.0040	0.00382		0.0045	0.0085	0.0048	0.0077	0.0049	0.0077	0.0038	0.0028	0.0026
O1	U_{11}	0.0136	0.0171	0.0186	0.0181	0.0198	0.0161	0.0264	0.0174	0.0330	0.0180	0.0175	0.0211
	U_{22}	0.0235	0.0225	0.0251	0.0279	0.0275	0.0251	0.0341	0.0247	0.0289	0.0249	0.0223	0.0284
	U_{33}	0.0182	0.0143	0.0215	0.0187	0.0227	0.0133	0.0303	0.0155	0.0255	0.0145	0.0184	0.0152
	U_{23}	-0.0035	-0.0027	-0.0020	-0.0041	-0.0036	-0.0025	-0.0047	-0.0026	-0.0009	-0.0030	-0.0018	-0.0015
	U_{13}	0.0051	0.0044	0.0048	0.0053	0.0076	0.0045	0.0081	0.0043	0.0075	0.0038	0.0044	0.0034
	U_{12}	-0.0067	-0.0057	-0.0062	-0.0092	-0.0066	-0.0053	-0.0079	-0.0067	-0.0056	-0.0059	-0.0049	-0.0048
O2	U_{11}	0.0245	0.0241	0.0282	0.0282	0.0295	0.0219	0.0364	0.0270	0.0346	0.0263	0.0234	0.0284
	U_{22}	0.0146	0.0130	0.0129	0.0136	0.0192	0.0163	0.0231	0.0133	0.0184	0.0144	0.0146	0.0207
	U_{33}	0.0160	0.0141	0.0207	0.0206	0.0219	0.0166	0.0279	0.0173	0.0352	0.0160	0.0176	0.0157
	U_{13}	0.0011	0.0004	0.0015	-0.0009	0.0026	0.0015	0.0009	-0.0012	0.0019	0.0007	-0.0012	0.0013
O3	U_{11}	0.0080	0.0092	0.0092	0.0134	0.0108	0.0076	0.0113	0.0083	0.0143	0.0079	0.0175	0.0063
	U_{22}	0.0097	0.0095	0.0091	0.0105	0.0100	0.0119	0.0074	0.0086	0.0136	0.0086	0.0170	0.0076
	U_{33}	0.0092	0.0104	0.0187	0.0074	0.0121	0.0088	0.0282	0.0101	0.0239	0.0110	0.0095	0.0108
	U_{23}	0.0005	0.0002	0.0009	0.0001	-0.0007	-0.0013	-0.0010	-0.0002	0.0013	0.0003	0.0003	-0.0005
	U_{13}	0.0011	0.0021	0.0019	0.0028	0.0043	0.0024	0.0041	0.0013	0.0056	0.0016	0.0012	0.0029
	U_{12}	-0.0011	-0.0003	0.0004	-0.0004	0.0002	0.0001	-0.0027	-0.0001	0.0035	0.0002	0.0004	-0.0001
O4	U_{11}	0.0064	0.0090	0.0092	0.0126	0.0113	0.0125	0.0139	0.0086	0.0127	0.0095	0.0170	0.0072
	U_{22}	0.0129	0.0124	0.0107	0.0131	0.0111	0.0152	0.0113	0.0104	0.0109	0.0118	0.0256	0.0096
	U_{33}	0.0094	0.0101	0.0183	0.0077	0.0141	0.0088	0.0272	0.0100	0.0397	0.0086	0.0099	0.0074
	U_{13}	0.0010	0.0012	0.0016	0.0022	0.0039	0.0003	0.0025	0.0025	0.0078	0.0002	0.0010	0.0006

literature data fall close to the trend defined by the data from this study. The octahedral flattening angles for M1 and M2 are very similar for the synthetic samples with Si_3Al tetrahedral composition investigated here. The preference of Al^{3+} for the M2 site, however, results in distinct differences between ψ_{M1} and ψ_{M2} for samples close to the annite-siderophyllite join with significant amounts of octahedral Al^{3+} (no. Sdp, no. Sd87).

The ratio of e_u/e_s (Toraya 1981) is related to polyhedral distortion. The terms e_u and e_s are the mean O-O bond lengths of the unshared and shared edges of the octahedron, respectively. In Figure 4a, e_u/e_s is plotted against the mean M-O bond lengths of the M1 and the M2 sites. The substitution of Fe^{2+} by smaller divalent cations in annite results in an increase of the difference between shared and unshared edge lengths of the octahedra and thus results in increasing of e_u/e_s with decreasing average M-O distances. As is the case for the octahedral flattening angle ψ , the changes in e_u/e_s vs. average M-O for the M1 and M2 sites are similar. Literature data of e_u/e_s vs. mean M2-O for the M2 site plot along the trend found for the synthetic samples with Si_3Al tetrahedral composition. Literature data for the M1 site show large scattering within a field limited

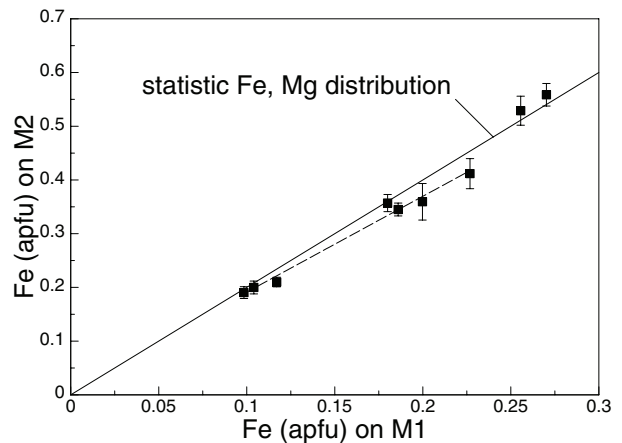


FIGURE 2. Cationic distribution of Fe and Mg at the M1 and M2 sites in the synthetic trioctahedral micas of the annite-phlogopite binary. The solid line represents equal distribution of Fe and Mg over M1 and M2. The dashed line is a linear regression curve through the data of this study except for the two data at high Fe concentrations.

TABLE 4b. Anisotropic atomic displacement factors U_{ij} (\AA^2) for the three natural trioctahedral 1//micas

	Ann#1	G-117	Sdp#3
T			
U_{11}	0.0105	0.0109	0.0112
U_{22}	0.0097	0.0108	0.0133
U_{33}	0.0118	0.0154	0.0168
U_{23}	-0.0001	-0.0002	-0.0001
U_{13}	0.0012	0.0029	0.0042
U_{12}	0.0002	-0.0006	-0.0001
M1			
U_{11}	0.0104	0.0094	0.0101
U_{22}	0.0087	0.0078	0.0111
U_{33}	0.0138	0.0144	0.0183
U_{13}	0.0025	0.0035	0.0046
M2			
U_{11}	0.0094	0.0086	0.0097
U_{22}	0.0095	0.0096	0.0123
U_{33}	0.0136	0.0133	0.0186
U_{13}	0.0009	0.0018	0.0039
K			
U_{11}	0.0420	0.0367	0.0367
U_{22}	0.0428	0.0379	0.0403
U_{33}	0.0317	0.0354	0.0302
U_{13}	0.0015	0.0067	0.0059
O1			
U_{11}	0.0290	0.0213	0.0219
U_{22}	0.0395	0.0289	0.0292
U_{33}	0.0190	0.0246	0.0232
U_{23}	-0.0022	-0.0036	-0.0030
U_{13}	0.0040	0.0062	0.0072
U_{12}	-0.0095	-0.0073	-0.0062
O2			
U_{11}	0.0417	0.0307	0.0272
U_{22}	0.0228	0.0145	0.0205
U_{33}	0.0208	0.0240	0.0242
U_{13}	0.0013	0.0017	0.0009
O3			
U_{11}	0.0143	0.0189	0.0211
U_{22}	0.0147	0.0174	0.0190
U_{33}	0.0154	0.0171	0.0205
U_{23}	-0.0001	0.0004	0.0005
U_{13}	0.0027	0.0022	0.0046
U_{12}	-0.0011	-0.0006	-0.0007
O4			
U_{11}	0.0159	0.0178	0.0184
U_{22}	0.0142	0.0222	0.0306
U_{33}	0.0203	0.0172	0.0217
U_{13}	0.0046	0.0018	0.0040

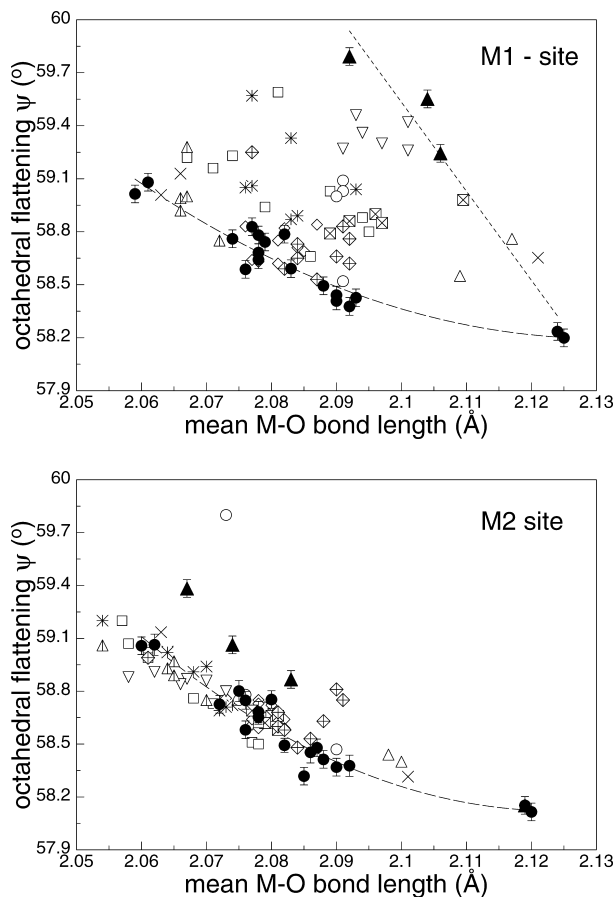
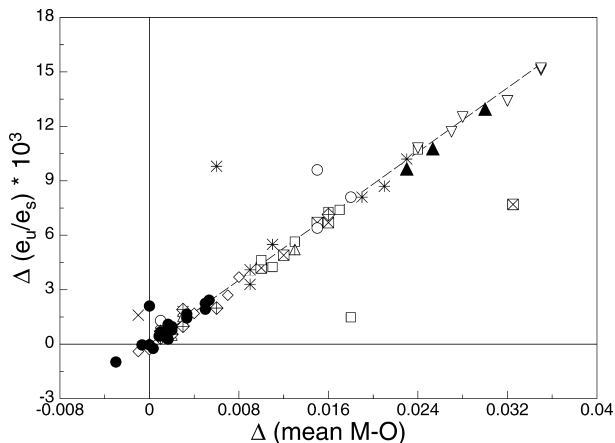
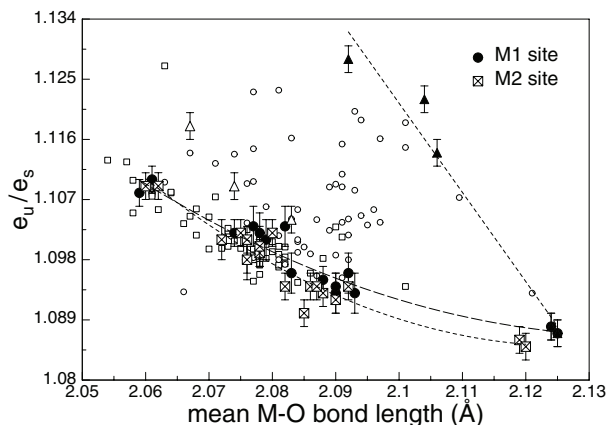
**FIGURE 3.** Variation of the octahedral flattening angle ψ (in degrees) with mean M1-O and mean M2-O bond lengths (in angstroms) for the M1 (a) and the M2 (b) sites. Symbols as in Figure 1. Lines fitted to the data are guides to the eye.**FIGURE 4.** (a) Relation between unshared/shared edge e_u/e_s of the octahedron vs. the mean M1-O and mean M2-O bond lengths for the synthetic micas with Si_3Al tetrahedral composition (filled circles and crossed squares = M1 and M2 site respectively) compared to the Fe^{2+} -, Al^{3+} -rich micas of the ann-sid join (filled and open triangles = M1 and M2 sites, respectively) and literature data (open circles and squares = M1 and M2 sites, respectively); (b) relation between $\Delta(e_u/e_s)$ [(= difference between $(e_u/e_s)_{\text{M1}}$ and $(e_u/e_s)_{\text{M2}}$] and $\Delta\langle\text{M-O}\rangle$ (= difference between mean M1-O-mean M2-O); symbols in (b) as in Figure 1; lines fitted to the data are guides to the eye.

TABLE 5A. Selected interatomic distances and parameters, derived from structure refinement of synthetic 1*M*/trioctahedral micas

	NiPhl#6	Phl#2	CoAn#2	Coni1.8#2	A20#2	A20#4	A40#7	A60#2	Mga1.2#1	Mga1.6#4	Sd87#4	GaPhl#1
M1-O4 (Å) ×2	2.038(2)	2.051(2)	2.063(2)	2.049(2)	2.057(2)	2.050(3)	2.063(3)	2.055(2)	2.060(2)	2.048(2)	2.086(2)	2.052(2)
M1-O3 (Å) ×4	2.070(2)	2.086(2)	2.101(2)	2.092(2)	2.089(2)	2.090(2)	2.104(2)	2.096(2)	2.110(2)	2.093(1)	2.095(1)	2.092(1)
mean M1-O (Å)	2.059	2.074	2.088	2.078	2.078	2.077	2.090	2.082	2.093	2.078	2.092	2.079
M2-O4 (Å)	2.051(3)	2.058(1)	2.075(2)	2.067(2)	2.064(2)	2.055(3)	2.068(3)	2.048(2)	2.062(2)	2.046(2)	2.063(2)	2.057(2)
M2-O3 (Å)	2.066(2)	2.074(1)	2.087(2)	2.083(1)	2.080(1)	2.083(2)	2.091(2)	2.095(2)	2.102(2)	2.091(1)	2.067(1)	2.079(2)
M2-O3 (Å)	2.070(3)	2.085(2)	2.100(2)	2.085(1)	2.091(2)	2.087(2)	2.096(2)	2.098(2)	2.106(2)	2.091(1)	2.070(1)	2.094(2)
mean M2-O (Å)	2.062	2.072	2.087	2.078	2.078	2.075	2.085	2.080	2.090	2.076	2.067	2.077
O4-H (Å)	0.91(4)	0.82(4)	0.96(4)	1.13(6)	0.87(4)	0.75(3)	0.84(5)	1.04(3)	0.91(5)	0.73(4)	0.99(4)	0.76(5)
ψ M1 (°)	59.01	58.76	58.49	58.64	58.68	58.83	58.41	58.79	58.43	58.78	59.79	58.66
ψ M2 (°)	59.06	58.73	58.48	58.65	58.68	58.80	58.32	58.75	58.37	58.75	59.38	58.63
e _u /e _s (M1)	1.108	1.102	1.095	1.099	1.100	1.103	1.093	1.103	1.093	1.102	1.128	1.099
e _u /e _s (M2)	1.109	1.101	1.094	1.099	1.100	1.102	1.090	1.102	1.092	1.101	1.118	1.170
BLD (M1) (%)	0.691	0.750	0.794	0.920	0.684	0.856	0.872	0.875	1.062	0.962	0.191	0.855
BLD (M2) (%)	0.366	0.461	0.412	0.364	0.460	0.643	0.544	1.036	0.893	0.963	0.118	0.631
ELD (M1) (%)	5.105	4.815	4.530	4.699	4.772	4.907	4.495	4.924	4.507	4.901	5.912	4.789
ELD (M2) (%)	5.075	4.632	4.346	4.590	4.613	4.698	4.186	4.677	4.218	4.653	5.337	7.655
OAV (M1) (°)	38.2	33.8	29.7	32.2	32.4	35.1	28.3	34.3	28.7	34.3	52.4	32.1
OAV (M2) (°)	38.9	33.8	30.0	32.4	32.8	34.9	27.2	34.1	28.1	34.0	45.0	31.8
T-O1 (Å)	1.668(2)	1.661(1)	1.662(2)	1.658(2)	1.661(2)	1.660(2)	1.655(2)	1.660(2)	1.663(2)	1.659(2)	1.670(2)	1.671(2)
T-O1 (Å)	1.649(2)	1.662(1)	1.659(2)	1.660(2)	1.662(2)	1.661(2)	1.659(2)	1.665(2)	1.666(2)	1.662(1)	1.672(2)	1.671(2)
T-O2 (Å)	1.657(1)	1.662(1)	1.660(1)	1.661(1)	1.663(2)	1.663(2)	1.659(2)	1.663(1)	1.663(1)	1.662(1)	1.670(2)	1.673(1)
T-O3 (Å)	1.656(2)	1.647(1)	1.657(2)	1.654(2)	1.653(2)	1.652(2)	1.646(2)	1.663(2)	1.642(2)	1.658(1)	1.697(2)	1.673(2)
mean T-O (Å)	1.658	1.658	1.660	1.658	1.660	1.659	1.655	1.663	1.659	1.660	1.677	1.672
α (°)	9.48	9.20	7.64	8.31	9.41	9.02	8.44	8.67	8.49	8.88	11.55	10.78
τ (°)	110.49	110.70	110.56	110.67	110.37	110.49	110.26	110.36	10.43	110.50	108.96	110.68
TAV (°)	1.3	1.9	1.5	1.8	1.0	1.3	0.8	1.0	1.1	1.3	0.3	1.8
BLD (%)	0.317	0.332	0.104	0.136	0.203	0.211	0.264	0.083	0.497	0.105	0.589	0.060
K-O1 (Å) ×4	2.961(2)	2.974(1)	3.015(2)	2.992(2)	2.976(2)	2.980(2)	2.995(2)	2.987(2)	2.991(2)	2.979(2)	2.943(2)	2.943(2)
K-O2 (Å) ×2	2.959(2)	2.972(1)	3.012(2)	2.987(2)	2.973(2)	2.979(2)	2.994(2)	2.985(2)	2.996(2)	2.976(2)	2.942(2)	2.943(2)
K-O1 (Å) ×4	3.397(2)	3.388(1)	3.358(2)	3.366(2)	3.397(2)	3.387(2)	3.375(2)	3.378(2)	3.377(2)	3.378(2)	3.465(2)	3.434(2)
K-O2 (Å) ×2	3.409(2)	3.392(1)	3.361(2)	3.371(2)	3.398(2)	3.390(2)	3.375(2)	3.389(2)	3.382(2)	3.385(2)	3.475(2)	3.436(2)
mean K-O _{inner} (Å)	2.958	2.973	3.014	2.990	2.975	2.980	2.995	2.986	2.993	2.978	2.943	2.943
mean K-O _{outer} (Å)	3.401	3.389	3.359	3.368	3.397	3.388	3.375	3.382	3.379	3.380	3.469	3.435
Δ<K-O> (Å)	0.443	0.416	0.345	0.377	0.422	0.408	0.380	0.395	0.386	0.402	0.526	0.492

Notes: ψ (octahedral flattening angle): $\cos \psi = \frac{t_o}{2d_o} - t_o = 2 \cdot \left(0.5 - \frac{2(z_{O3} + z_{O4})}{3} \right) \cdot c \sin \beta$ d_o = average M-O distance, t_o = octahedral sheet thickness, z_{O3} and z_{O4} fractional z coordinates of O3 and O4 O atoms respectively (Hazen and Burnham 1973); e_u, e_s = mean lengths of unshared and shared octahedral edges, respectively (Toraya 1981); BLD (bond length distortion) = $\frac{100}{n} \sum_{i=1}^n \frac{|(X-O)_i - \langle X-O \rangle|}{\langle X-O \rangle}$ where n is the number of bonds and (X-O) is the central cation-O atom length (Renner and Lehmann 1986), ELD (edge length distortion) = $\frac{100}{n} \sum_{i=1}^n \frac{|(O-O)_i - \langle O-O \rangle|}{\langle O-O \rangle}$ where n is the number of bonds and (O-O) is the polyhedron edge length (Renner and Lehmann 1986); OAV (octahedral angle variance) = $\sum_{i=1}^3 (\theta_i - 90) / 11$ (Robinson et al. 1971); α (tetrahedral rotation angle): $\tan \alpha = 4\sqrt{3}(0.25 - \gamma_{OT})$ (Hazen and Burnham 1973), τ (tetrahedral flattening angle) = $\sum_{i=1}^3 (O_{\text{basal}} - T - O_{\text{apical}}) / 3$; TAV (tetrahedral angle variance) = $\sum_{i=1}^3 (\theta_i - 109.47) / 5$ (Robinson et al. 1971); Δ<K-O> = <K-O_{outer}> - <K-O_{inner}>

by the e_u/e_s vs. mean M1-O data for micas near the annite-siderophyllite join. The M1 site in Al³⁺ substituted micas shows a larger deviation from ideal octahedral geometry as compared to the M2 site. The distortion increases with increasing octahedral Al³⁺ content. The difference between e_u/e_s for M1 and for M2 (Δe_u/e_s) is small for the micas of this study with a tetrahedral composition of Si₃Al and do not change systematically with the size of the octahedral cation. These observations are similar for the difference Δ<M-O> = mean M1-O - mean M2-O.

Brigatti and Davoli (1990) found a close correlation (Fig. 4b) between Δe_u/e_s vs. Δ<M-O>. Filled circles and squares are data from this study and reflect the small difference between the M1 and M2 sites for micas of Si₃Al tetrahedral composition. There is an increasing difference between M1 and M2 with increasing Al³⁺ content (samples close to the ann-sid join,

filled squares). The Fe²⁺, Al³⁺-rich micas of Brigatti et al. (2000a, b) exhibit the largest differences between the M1 and M2 sites in terms of Δe_u/e_s vs. Δ<M-O>. Brigatti and Davoli (1990) also observed that phlogopite crystals, biotite crystals, and annite crystals plot to well-defined fields and this observation is consistent with more recent data (after 1990, Fig. 4b). Although this behavior is consistent with increasing Fe²⁺ content, we suggest that octahedral Al³⁺ may be a major factor in making the M1 and M2 sites more distinct, because natural Fe-rich micas tend to have greater octahedral Al³⁺ concentrations as compared to natural phlogopite crystals. Note that the data for the Al³⁺-poor micas of Brigatti et al. (2001) plot at low Δe_u/e_s vs. Δ<M-O> values similar to those for the synthetic trioctahedral micas with Si₃Al tetrahedral composition of this study.

As shown by Toraya (1981), octahedral flattening ψ and e_u/

TABLE 5b. Selected interatomic distances and parameters, derived from structure refinement of the three natural 1M trioctahedral micas

	Ann#1	G-117	Sdp#3
M1-O4 (Å) ×2	2.119(1)	2.095(2)	2.096(2)
M1-O3 (Å) ×4	2.127(1)	2.111(2)	2.108(2)
mean M1-O (Å)	2.124	2.106	2.104
M2-O4 (Å)	2.107(1)	2.073(2)	2.067(2)
M2-O3 (Å)	2.122(1)	2.084(2)	2.075(2)
M2-O3 (Å)	2.129(1)	2.091(2)	2.080(2)
mean M2-O (Å)	2.119	2.083	2.074
O4-H (Å)	0.81(4)	0.94(3)	0.74(5)
ψ M1 (°)	58.25	59.24	59.55
ψ M2 (°)	58.15	58.87	59.07
e _u /e _s (M1)	1.088	1.114	1.122
e _u /e _s (M2)	1.086	1.104	1.109
BLD (M1) (%)	0.167	0.338	0.253
BLD (M2) (%)	0.388	0.309	0.225
ELD (M1) (%)	4.118	5.331	5.640
ELD (M2) (%)	3.964	4.740	4.917
OAV (M1) (°)	25.7	41.9	48.0
OAV (M2) (°)	24.9	36.0	39.6
T-O1 (Å)	1.661(1)	1.666(2)	1.665(1)
T-O1 (Å)	1.669(1)	1.666(1)	1.667(1)
T-O2 (Å)	1.666(1)	1.665(2)	1.666(1)
T-O3 (Å)	1.664(1)	1.683(2)	1.681(1)
mean T-O (Å)	1.665	1.670	1.670
α (°)	2.55	7.99	8.66
τ (°)	110.28	109.82	109.70
TAV (°)	0.8	0.2	0.1
BLD (%)	0.150	0.389	0.337
K-O1 (Å) ×4	3.149(2)	3.010(2)	2.994(2)
K-O2 (Å) ×2	3.116(2)	3.004(2)	2.991(2)
K-O1 (Å) ×4	3.245(2)	3.371(2)	3.386(2)
K-O2 (Å) ×2	3.276(2)	3.390(2)	3.402(2)
mean K-O _{inner} (Å)	3.138	3.008	2.993
mean K-O _{outer} (Å)	3.255	3.377	3.391
Δ<K-O> (Å)	0.117	0.369	0.398

Notes: Abbreviations as in Table 5A.

e_s also are highly correlated. Octahedra in annite are closer to the ideal geometry as compared to “Ni-phlogopite.” Furthermore, distortions of the M1 and M2 sites are similar for the data of this study, but less so for the literature data. Data of e_u/

e_s vs. ψ for the M1 site plot at intermediate-to-high e_u/e_s vs. ψ values along a linear regression line, and data for the M2 site plot at low-to-intermediate values. The largest deviation from ideal octahedral geometry is observed for the M1 site of sample no. Sd87, richest in octahedrally coordinated Al³⁺.

With respect to bond length distortion (BLD), the M1 and M2 octahedra of the micas investigated here are regular. The deviation of individual bond lengths from the mean is less than 1% for all samples for both M1 and M2 sites. There is no systematic variation of BLD as a function of chemical composition. The only trend observable is a slightly smaller BLD for the M2 site as compared to the M1 site. The edge lengths distortion (ELD) shows an inverse correlation (Fig. 5) with mean M1-O and mean M2-O bond lengths. Annite shows the smallest deviation of individual O-O edge lengths from the mean O-O edge lengths, “Ni-phlogopite” shows the largest. Excluding the data for near end-member annite, the variation of ELD with mean M1-O and mean M2-O is nearly linear and ELD_{M1} and ELD_{M2} are similar within experimental error. The quadratic octahedral-angle variance (OAV) also shows (Fig. 6) an inverse correlation with the mean M1-O and mean M2-O bond lengths. Data points for the M1 and M2 sites are close together and, excluding the data for annite, a linear decrease of OAV with increasing mean M1-O and mean M2-O bond lengths is observed for the micas with tetrahedral Si₃Al composition.

The distortion parameters show that the octahedra in annite have the smallest deviation from ideal octahedral geometry, whereas in “Ni-phlogopite,” which contains the smallest octahedral cation, the octahedral sheet is most distorted among all the micas with tetrahedral Si₃Al composition investigated in this study. In contrast to literature data, the M1 and M2 sites are very similar in terms of site distortion.

Tetrahedral sheet and interlayer site

The deviation of individual T-O bond lengths from their mean value is <0.3%. There is no systematic change of BLD with chemical composition. The O-T-O bond angles also are close to the ideal value of 109.47° (Table 5). The O_{basal}-T-O_{apical}

TABLE 6a. Al content (apfu) and Fe and Al cationic distribution at the M1 and M2 sites for the Fe²⁺-, Al³⁺-rich micas close to the annite-siderophyllite join

Sample	Fe (EMP)*	Al (EMP)†	Al† (X-ray)	Al† (M1)	Al† (M2)	<r _{oct} >
G-117	2.42	0.38	0.446(8)	0.123	0.323	0.7293
Sdp#3	2.17	0.71	0.699(7)	0.180	0.519	0.7183
Sd87#4	2.18	0.79	0.822(8)	0.204	0.618	0.7120

Note: EMP = from electron microprobe analysis.

* Fe content also includes Mn content as in structure refinement the occupancy of M1 and M2 was refined as Fe + Mn because of close similarity of atomic scattering factors.

† Al content also includes Mg content as the occupancy of M1 and M2 was refined as Al + Mg because of close similarity of atomic scattering factors.

TABLE 6b. Fe content (apfu) and Fe and Mg cationic distribution at the M1 and M2 sites for micas of the annite-phlogopite solid-solution

Sample	Fe (EMP)	Al ⁽⁶⁾ (EMP)	Fe (X-ray)	Fe (M1)	Fe (M2)	<r _{oct} >
A20#2	0.33(1)	—	0.327(7)	0.117	0.210	0.7265
A20#4	0.33(1)	—	0.304(7)	0.104	0.200	0.7261
A40#7	0.53(3)	—	0.537(6)	0.180	0.357	0.7307
A60#2	0.68(1)	—	0.531(7)	0.186	0.345	0.7306
A80#1	0.56(2)	0.054(2)	0.559(8)	0.200	0.359	0.7278
A80#2	0.68(3)	0.059(2)	0.639(7)	0.227	0.412	0.7290
Mga1.2#1	0.82(3)	—	0.785(7)	0.256	0.529	0.7357
Mga1.2#4	0.82(3)	—	0.829(7)	0.270	0.559	0.7366
Mga1.6#4	0.50(1)	—	0.289(7)	0.098	0.191	0.7258

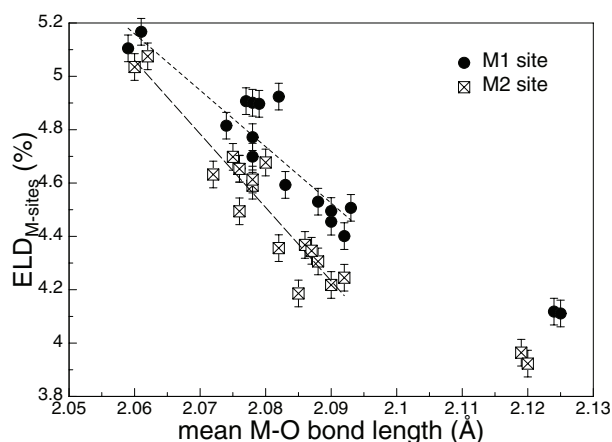


FIGURE 5. Relation between the edge length distortion ELD parameter (Renner and Lehmann 1986) and mean M1-O and mean M2-O bond length for the synthetic micas with Si_3Al tetrahedral composition; lines fitted to the data are guides to the eye.

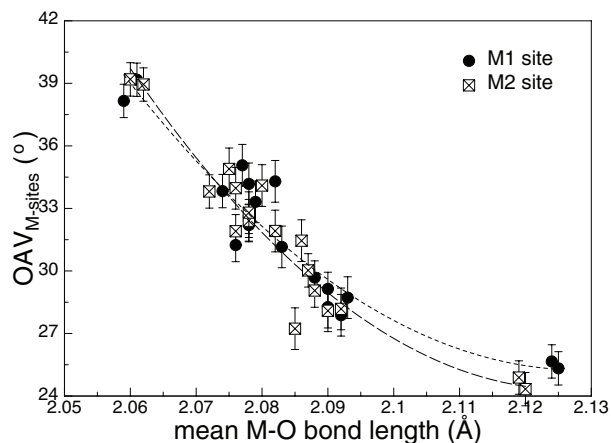


FIGURE 6. Relation between the octahedral angle variation OAV parameter (Renner and Lehmann 1986) and mean M1-O and mean M2-O bond length for the synthetic micas with Si_3Al tetrahedral composition; lines fitted to the data are guides to the eye.

angles (τ) are slightly larger than the ideal values (110.0–110.7°; Table 5), and thus the angles $\text{O}_{\text{basal}}\text{-T-O}_{\text{basal}}$ are slightly smaller than ideal. There are no systematic variations of tetrahedral bond angles or tetrahedral distortion parameters (BLD, TAV) with the chemical composition of the octahedral sheet for micas with tetrahedral Si_3Al composition. The τ value varies between 110.3 and 110.7° for the micas with Si_3Al tetrahedra, which are elongated along \mathbf{c}^* . For the micas near the annite-siderophyllite join, τ decreases almost linearly with increasing tetrahedral Al^{3+} and is 109.0(1)° in sample no. Sd87, i.e., the tetrahedra become more flattened. The tetrahedral-angle variance (TAV) is $<2^\circ$ for all samples investigated. Figure 7 displays the variation of the mean T-O bond length with chemical composition of the octahedral sheet. Data from literature are included and these do not show a trend with mean M1-O and mean M2-O bond lengths. Mean T-O bond lengths from this study suggest a small increase with increasing mean M1-O and

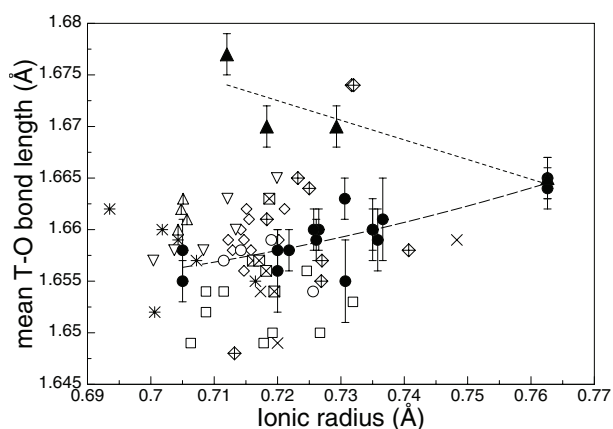


FIGURE 7. Relation between mean octahedral ionic radius and mean T-O bond lengths. Symbols as in Figure 1; lines fitted to the data are guides to the eye.

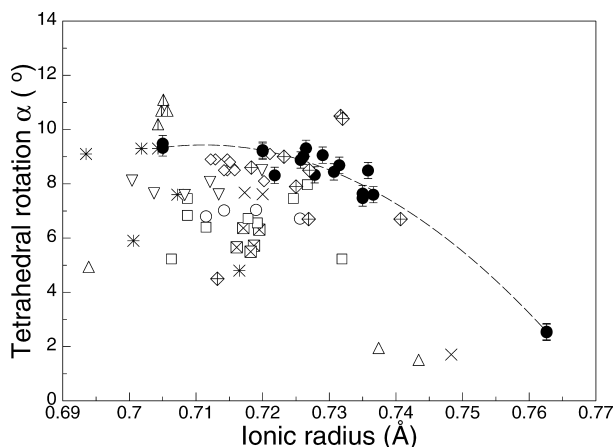


FIGURE 8. Relation between the tetrahedral rotation angle α and the mean octahedral ionic radius; Symbols as in Figure 1; lines fitted to the data are guides to the eye.

mean M2-O, similar to the results of Brigatti and Davoli (1990). The increase of mean T-O for the Fe^{2+} -, Al^{3+} -rich micas on the annite-siderophyllite binary, which is more evident, is related to the incorporation of the larger tetrahedral Al^{3+} cation through the coupled substitution $^{6}\text{Fe}^{2+} + ^{4}\text{Si}^{4+} \rightarrow ^{6}\text{Al}^{3+} + ^{4}\text{Al}^{3+}$.

The main mechanism in matching the lateral dimensions of the octahedral and tetrahedral sheets is octahedral flattening (ψ) and ditrigonal distortion (α) of the tetrahedral sheet (Donnay et al. 1964). Whereas in annite, individual tetrahedra are nearly in ideal hexagonal arrangement ($\alpha = 2.5^\circ$), ditrigonal distortion increases with decreasing mean octahedral ionic radius (Fig. 8). As our data show only “simple” chemical composition and no multiple cationic substitutions, e.g., as compared to natural trioctahedral *1M* micas, a correlation between α vs. the mean octahedral ionic radius (or average M-O) does exist for our data. The data suggest that for K-rich micas and Si_3Al

tetrahedral composition, a tetrahedral rotation angle of about 9.5° seems to be an upper limit. For Fe^{2+} -, Al^{3+} -rich micas, larger values of α are possible. Sample no. Sd87 exhibit a ditrigonal distortion of $\alpha = 11.6^\circ$, which is among the highest values reported for 1M true trioctahedral micas so far.

"Tetra-gallium-phlogopite" $\text{KMg}_3\text{Si}_3\text{GaO}_{10}(\text{OH})_2$ was synthesized as well; lattice parameters and structural details are included in Tables 3–5. The octahedral distortion parameters are comparable to those of phlogopite. The main differences between the Ga-rich phlogopite and phlogopite are the T-O bond lengths because of the Ga^{3+} ($r = 0.47 \text{ \AA}$; Shannon 1970). Because the Ga-rich phlogopite has a large tetrahedral sheet but a similar octahedral sheet, $\text{KMg}_3\text{Si}_3\text{GaO}_{10}(\text{OH})_2$ has a larger ditrigonal distortion of $\alpha = 10.8^\circ$ (cf. phlogopite, $\alpha = 9.2^\circ$).

ACKNOWLEDGMENTS

G.J.R. thanks the Alexander von Humboldt-Stiftung for support in 1998–1999, when he was a Humboldt Fellow at the Institute of Crystallography at the RWTH in Aachen. This study was supported financially by the Austrian Academy of Science through an APART (Austrian Program for Advanced Research and Technology) fellowship to G.J.R., which is gratefully acknowledged. We thank A. Lalonde for making available the two natural samples of "Ann" and "Sdp," and M.D. Dyar for generously providing us with material and chemical composition of the Barker biotite G-117. J. Ernst (RWTH Aachen) tirelessly helped with the high-temperature/high-pressure experiments, and M. Bernroider helped with electronmicroprobe analysis. The paper benefited from the constructive and detailed reviews of S. Guggenheim, L. Medici, and the Associate Editor M.F. Brigatti.

REFERENCES CITED

- Alietti, E., Brigatti, and M.F., Poppi, L. (1995) The crystal structure and chemistry of high-aluminum phlogopite. *Mineralogical Magazine*, 59, 149–157.
- Brigatti, M.F. and Davoli, P. (1990) Crystal-structure refinements of 1M plutonic biotites. *American Mineralogist*, 75, 305–313.
- Brigatti, M.F. and Poppi, L. (1993) Crystal chemistry of Ba-rich trioctahedral micas—1M. *European Journal of Mineralogy*, 5, 857–871.
- Brigatti, M.F., Galli, E., and Poppi, L. (1991) Effect of Ti substitution in biotite—1M crystal chemistry. *American Mineralogist*, 76, 1174–1183.
- Brigatti, M.F., Medici, L., Sacconi, E., and Vaccaro, C. (1996a) Crystal chemistry and petrologic significance of Fe^{3+} -rich phlogopite from the Tapira carbonatite complex, Brazil. *American Mineralogist*, 81, 913–927.
- Brigatti, M.F., Medici, L., and Poppi, L. (1996b) Refinement of the structure of natural ferriphlogopite. *Clays and Clay Minerals*, 44, 540–545.
- Brigatti, M.F., Lugli, C., Poppi, L., and Elburg, M. (1998) Crystal chemistry of biotites from mafic enclaves in the Warburton granodiorite, Lachlan Fold Belt (Australia). *European Journal of Mineralogy*, 10, 855–864.
- Brigatti, M.F., Frigieri, P., Ghezzi, C., and Poppi, L. (2000a) Crystal chemistry of Al-rich biotites coexisting with muscovite in peraluminous granites. *American Mineralogist*, 85, 436–448.
- Brigatti, M.F., Lugli, C., Poppi, L., Foord, E.E., and Kile, D.E. (2000b) Crystal chemical variations in Li- and Fe-rich micas from Pikes Peak batholith (central Colorado). *American Mineralogist*, 85, 1275–1286.
- Brigatti, M.F., Medici, L., Poppi, L., and Vaccaro, C. (2001) Crystal chemistry of trioctahedral micas-1M from the Alto Paranaíba Igneous Province, Southeastern Brazil. *Canadian Mineralogist*, 39, 1333–1345.
- Comodi, P., Zanazzi, P.F., Weiss, Z., Rieder, M., and Drabek, M. (1999) "Cs-tetraferri-annite": High-pressure and high-temperature behavior of a potential nuclear waste disposal phase. *American Mineralogist*, 84, 325–332.
- Cruciani, G. and Zanazzi, P.F. (1994) Cation partitioning and substitution mechanisms in 1M phlogopite: A crystal chemical study. *American Mineralogist*, 79, 289–301.
- Donnay, G., Morimoto, N., Takeda, H., and Donnay, J.H.D. (1964) Trioctahedral one-layer micas: I. Crystal structure of a synthetic iron mica. *Acta Crystallographica*, 17, 1369–1373.
- Guggenheim, S. and Eggleton, R.A. (1987) Modulated 2:1 layer silicates: Review, systematic, and predictions. *American Mineralogist*, 72, 724–738.
- Hamilton, D.L. and Henderson, C.M.B. (1968) The preparation of silicate compositions by a gelling method. *Mineralogical Magazine*, 35, 832–838.
- Hazen, R.M. and Burnham, C.W. (1973) The crystal structure of one-layer phlogopite and annite. *American Mineralogist*, 58, 889–900.
- Hazen, R.M. and Wones, D.R. (1972) The effect of cationic substitutions on the physical properties of trioctahedral micas. *American Mineralogist*, 57, 103–129.
- Hewitt, D.A. and Wones, D.R. (1975) Physical properties of some Fe-Mg-Al trioctahedral biotites. *American Mineralogist*, 60, 854–862.
- Joswig, W. (1972) Neutronenbeugungsmessungen an einem 1M Phlogopit. *Neues Jahrbuch für Mineralogie Monatshefte*, 1–11.
- Lalonde, A.E., Rancourt, D.G., and Chao, G.Y. (1996) Fe-bearing trioctahedral micas from Mont Saint-Hilaire, Quebec. *Mineralogical Journal*, 60, 447–460.
- McCaughey, J.W., Newnham, R.E., and Gibbs, G.V. (1973) The crystal structure of synthetic fluorophlogopite. *American Mineralogist*, 58, 249–254.
- Nelson, D.O. and Guggenheim, S. (1993) Inferred limitations to the oxidation of Fe in chlorite: A high temperature single-crystal X-ray study. *American Mineralogist*, 78, 1197–1207.
- Rancourt, D.G., Ping, J.Y., and Berman, R.G. (1994) Mössbauer spectroscopy of minerals III. Octahedral-site Fe^{2+} quadrupole splitting distributions in layer silicates. *Physics and Chemistry of Minerals*, 21, 258–267.
- Rancourt, D.G., Ping, J.Y., Boukili, B., and Robert, J.L. (1996) Octahedral-site Fe^{2+} quadrupole splitting distributions from Mössbauer spectroscopy along (OH, F)-annite join. *Physics and Chemistry of Minerals*, 23, 63–71.
- Redhammer, G.J. (1998) Characterization of synthetic trioctahedral micas by Mössbauer spectroscopy. In D.G. Rancourt, Ed., *Mössbauer spectroscopy in Clay Science*. ICC'97 special Issue, *Hyperfine Interactions*, 117, 85–115.
- (2001) Kontrollierte chemische Substitutionen in ausgewählten Ketten- und Schichtsilikaten: Beiträge von Mössbauerspektroskopie und Einkristall-Röntgenbeugung zu Kristallstruktur, Kristallchemie und Magnetismus von Glimmern und Klinopyroxenen. *Habilitation Thesis*. 335 p., Rheinisch-Westfälische Technische Hochschule (RWTH) Aachen, Germany (in German).
- Redhammer, G.J., Beran, A., Dachs, E., and Amthauer, G. (1993) A Mössbauer and X-ray diffraction study of annites synthesized at different oxygen fugacities and crystal chemical implications. *Physics and Chemistry of Minerals*, 20, 382–394.
- Redhammer, G.J., Dachs, E., and Amthauer, G. (1995) Mössbauer spectroscopic and X-ray powder diffraction studies of synthetic micas on the join $\text{KFe}_3\text{AlSi}_3\text{O}_{10}(\text{OH})_2$ -phlogopite $\text{KMg}_3\text{AlSi}_3\text{O}_{10}(\text{OH})_2$. *Physics and Chemistry of Minerals*, 22, 282–294.
- Redhammer, G.J., Beran, A., Schneider, J., Amthauer, G., and Lottermoser, W. (2000) Spectroscopic and structural properties of synthetic micas on the annite-siderophyllite binary $\{ \text{K} \} [\text{Fe}^{2+}_3] < \text{AlSi}_3 > \text{O}_{10}(\text{OH})_2 - \{ \text{K} \} [\text{Fe}^{2+}_2\text{Al}] < \text{Al}_2\text{Si}_2 > \text{O}_{10}(\text{OH})_2$. *American Mineralogist*, 85, 449–465.
- Renner, B. and Lehmann, G. (1986) Correlation of angular and bond lengths distortion in TO₂ units in crystals. *Zeitschrift für Kristallographie*, 175, 43–59.
- Robinson, K., Gibbs, G.V., and Ribbe, P.H. (1971) Quadratic elongation, a quantitative measure of distortion in coordination polyhedra. *Science*, 172, 567–570.
- Shannon R.D. (1970) Revised values of effective ionic radii. *Acta Crystallographica*, B26, 1046–1048.
- Sheldrick, G. (1997) SHELXL, a program for refining crystal structures. University of Göttingen.
- Stoe and Cie (1996) X-SHAPE and X-RED: programs for optimizing of the crystal shape (w.r.t. the merging R-value) and numerical absorption correction. Stoe GesmbH, Darmstadt, Germany.
- Toraya, H. (1981) Distortions of octahedra and octahedral sheets in 1M micas and the relation to their stability. *Zeitschrift für Kristallographie*, 157, 173–190.

MANUSCRIPT RECEIVED JANUARY 15, 2002

MANUSCRIPT ACCEPTED JUNE 18, 2002

MANUSCRIPT HANDLED BY MARIA FRANCA BRIGATTI